한국소음진동공학회 창립10주년 기념 소음진동학술대회논문집, pp. 606~611.

ENHANCEMENT THE SOUND TRANSMISSION LOSS OF POROELASTIC LININGS

°B. Heukjin Song* and J. Stuart Bolton**

ABSTRACT

It has been noted that the low frequency absorption coefficient of a porous sample placed in a standing wave tube is affected by the nature of the sample's edge constraint. The edge constraint has the effect of stiffening the solid phase of the sample, which itself can be strongly coupled to the material's fluid phase, and hence the incident sound field, by viscous means at low frequencies. In recent work it has also been shown that such a circumferential constraint causes the low frequency transmission loss of a layer of fibrous material to approach a finite low frequency limit that is proportional to the flow resistance of the layer and which is substantially higher than that of an unconstrained sample of the same material. However, it was also found that the benefit of the circumferential edge constraint was reduced in a transitional frequency range by a shearing resonance of the sample. Here it will be shown that the effect of that resonance can be mitigated or eliminated by adding additional axial and radial constraints running through the sample. It will also be shown that the constraint effect can be modeled closely by using a finite element procedure based on the Biot poroelastic theory. Implications for low frequency barrier design are also discussed.

1. INTRODUCTION

Recently, a transfer matrix, standing wave tube method for estimating the complex wave number and characteristic impedance of porous materials has been developed [1]. By using a similar procedure it was possible to measure the transmission loss of aviation-grade glass fiber samples (2.9 cm in diameter and 7.5 cm in depth) from 100 Hz to 6400 Hz. The transmission losses of these materials consistently showed resonance dips in the 400 Hz to 500 Hz range: it was suggested that the dips resulted from a shearing resonance of the sample mass against the edge constraint of the samples when placed in the standing wave tube. It has been verified that the circumferential edge-constraint effects described above can be successfully modeled by using an axi-symmetric finite element procedure [2] based on the Biot poroelastic theory [3]. The focus of the present work was on the enhancement of the increased transmission loss that was found to occur at frequencies below the shearing resonance. That is, the transmission loss was enhanced at low frequencies due to sample edge constraint. The most important findings of the present work are that: the shearing resonance dips can be shifted to higher frequencies; the impact of the resonance dips can be reduced; and hence the transmission loss of a fibrous layer can be increased at low frequencies by applying a variety of internal axial and radial constraints within the sample.

2. EXPERIMENTAL APPARATUS

In the work described here, a 10 cm inner diameter, low frequency standing wave tube was used to measure the anechoic transmission loss and surface normal impedance of the various samples [1]. The tube was modified by the addition of four, custom-made sections (see Fig. 1). One of the additional tube sections was drilled to accommodate three microphone holders. In the present work, the

* Ray W. Herrick Lab., School of Mechanical Engineering, Purdue University: Graduate Research Assistant

** Ray W. Herrick Lab., School of Mechanical Engineering, Purdue University: Professor

two microphone locations used in both the up- and downstream tube sections were separated by 5 cm; measurement position 2 was located 35 cm from the front surface of the sample, and measurement position 3 was located 25 cm from the rear surface of the sample.

The material considered here was aviation-grade glass fiber. The properties of this material, inferred by a combination of direct measurement and model matching, are listed in Table 1. In all cases, the diameter of the samples was 10 cm and the sample depth was 7.5 cm (each sample comprising three, 2.5 cm thick layers). Here, different types of internal constraints were applied by using thin plexiglasss sheets (7.5 cm in length) running in the axial and radial directions through the samples. In particular, the samples were either constrained along a plane (see Fig. 3 (a)) or constrained within a cross (see Fig. 4 (a)). In the reference case, the sample was constrained only around its circumference (see Fig. 2 (a)). Note that the samples were constrained only by the effect of friction: i.e., no adhesives were used. The glass fiber samples were cut appropriately and then inserted carefully into the plexiglass frame within the sample holder. The anechoic termination in the large tube comprised a 60 cm depth of 3M Thinsulate material. The absorption coefficient of this termination was greater than 0.93 from 50 Hz to 1600 Hz. The anechoic termination was effective owing both to its length and because the absorbing material was packed loosely near the termination's front surface, and was more densely packed towards it downstream end.

The frequency span of the measurement was 1600 Hz and the frequency resolution was 2 Hz. In addition, a microphone switching calibration procedure that was based on the ASTM E 1050-90 two-microphone standing wave tube standard was used [4].

3. FINITE ELEMENT MODELS

The acoustical performance of the cylindrical glass fiber samples was modeled by using the code COMET/Acoustics–SAFE (supplied by Automated Analysis Corporation of Ann Arbor, Michigan). This software is based on a finite element implementation of the Biot theory for wave propagation in elastic porous materials [3]. More specifically, it is based on the version of the Biot theory described by Bolton et al. [5].

Here, the model comprised 540 poroelastic elements and 2160 air elements for a total of 2700 elements having 3146 nodes. All of the elements in the finite element model were three-dimensional acoustical fluid elements (ANSYS Fluid 30). This element is normally used for modeling the fluid medium in sound propagation problems. Each element had eight corner nodes. The parameters that were used to specify the properties of the poroelastic medium were: flow resistivity, tortuosity, porosity, bulk density of the expanded material, bulk *in vacuo* Young's modulus and corresponding loss factor, and Poisson's ratio.

In the air regions, the radial particle velocity was set to zero at the outer duct radius. In the poroelastic region, both the fluid and solid phase radial displacements were set to zero at the outer radius. The sample edge constraint was modeled by requiring that the axial solid phase velocity be zero along the surface of contact between the glass fiber and the duct wall. Similarly the fluid and solid phase normal displacements, and solid phase axial displacement, were set to zero on the planes of contact between the plexiglass and the glass fiber material. The lengths of the air spaces in the upstream and downstream sections were 15 cm each. The transfer matrix method was used to calculate the anechoic transmission loss and surface normal impedance of each "sample." Measurement position 2 was 10 cm from the front surface of sample and measurement position 1 was placed at the upstream end of the tube where a plane piston (having a unit axial velocity) was assumed to be located. Measurement position 3 was 10 cm from the rear surface of sample and measurement position 4 was placed at the anechoic termination. The right hand end of the air space was terminated by a $\rho_0 c$ impedance (i.e., a normalized impedance of unity), thus creating an anechoic termination. To make the FEM program run efficiently, the total number of elements should be small, and so the size of the elements was made equivalent to a quarter wavelength (of the lowest wave speed within the porous medium) at the highest frequency of interest.

4. RESULTS AND DISCUSSION

It was found that the major effect of the edge-constraint was to stiffen the sample at low frequencies: i.e., the reactances shown in Figs. 2 (b) to 4 (b) conform more closely to the constrained than the unconstrained predictions. It may be seen that the edge constraint transforms the low frequency behavior of the material from mass-like (i.e., a positive reactance) to spring-like (i.e., a negative reactance). The spring-like effect of the edge constraint also causes the incident sound field to experience increased resistance at low frequencies compared to the unconstrained case (when the material is free to move with the sound field). This effect is responsible for the increased low frequency resistance of the constrained case when compared to the unconstrained case.

The locations of the transmission loss resonance dips (at which the first axial shearing mode occurs) were well-predicted in the FEM results: see Figs. 2 (a) to 4 (a). The measured and predicted transmission loss results for the various constrained cases are shown together in Fig. 5. Note that the resonance dips shift to a progressively higher frequency as the degree of internal constraint is increased: in addition, the cross constraint essentially eliminates the resonance dip.

It was found that the low frequency limit of the transmission loss of the constrained samples was controlled by the material's flow resistivity as in the case of a rigid porous material: see Fig. 6. When the material has a relatively high flow resistivity, as in the present case, the transmission loss in the flow resistivity-controlled, low frequency region can be well in excess of that predicted on the basis of the material's mass per unit area. It is possible that this effect can be used to enhance the low frequency transmission loss of lined barriers if the linings are divided into small constrained segments as considered here. Thus the current findings have practical implications for the design of low frequency noise control barriers.

For example, the normal incidence transmission loss of a double panel system lined with 7.5 cm deep glass fiber materials for both internally constrained and unconstrained cases are shown in Fig. 7. Here, the thickness of the aluminum panels (ρ=2700 Kg/m^3) was 0.762 mm and the air gap between the panels and lining on both the incident and transmitted sides was 1 cm. Here, the "constrained" transmission loss was based on the use of transfer matrix elements measured using a small tube (2.9 cm diameter, edge-constrained samples). Those results are compared with the unconstrained transmission loss calculated for the unbonded-unbonded case [5]. These results show that the transmission loss of lined panel systems can be substantially increased at low frequencies (below 1000 Hz) by applying constraints within the lining material.

5. REFERENCES

1. B.H. Song and J.S. Bolton, "A transfer matrix approach for estimating the characteristic impedance and wave number of limp and rigid porous materials," *J. Acoust. Soc. Am.*, **107**, 1131-1152 (2000).
2. B. H. Song, J. S. Bolton and Y. J. Kang, "Effect of circumferential edge constraint on the transmission loss of glass fiber materials," *Inter-Noise 99*, 419-424 (1999).
3. M.A. Biot, "Theory of propagation of elastic waves in a fluid-saturated porous solid I. Low frequency range. II. Higher frequency range," *J. Acoust. Soc. Am.*, **28**, 168-191 (1956).
4. ASTM Standard E 1050-90, "Standard test method for impedance and absorption of acoustical materials using a tube, two microphones, and a digital frequency analysis system," (1990).
5. J.S. Bolton, N.-M. Shiau and Y.J. Kang, "Sound transmission through multi-panel structures lined with elastic porous materials," *J. Sound Vib.*, **191**, 317-347 (1996).

	Density [Kg/m]	Porosity	Tortuosity	Flow Resistivity [MKS Rayls / m]	Young's Modulus [Pa]	Poisson's ratio	Loss factor
Sample B	9.61	0.99	1.1	40000	8250	0.45	0.5

Table 1. Material properties of glass fiber material.

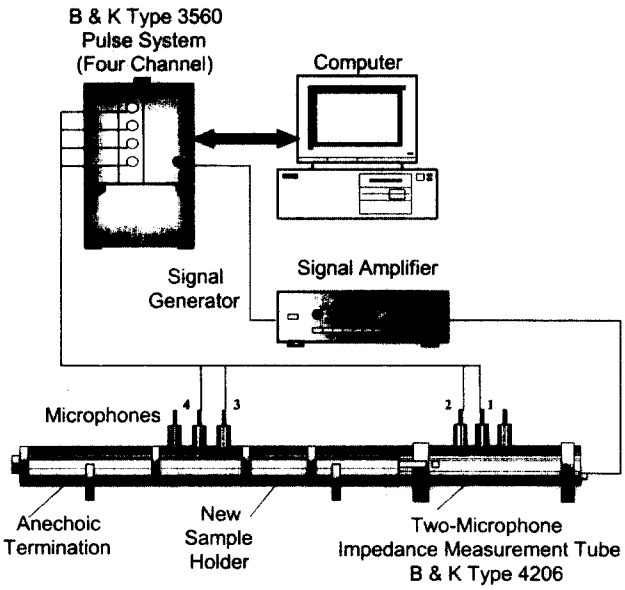

Figure 1. Experimental setup for low frequency measurements (10 cm inner diameter).

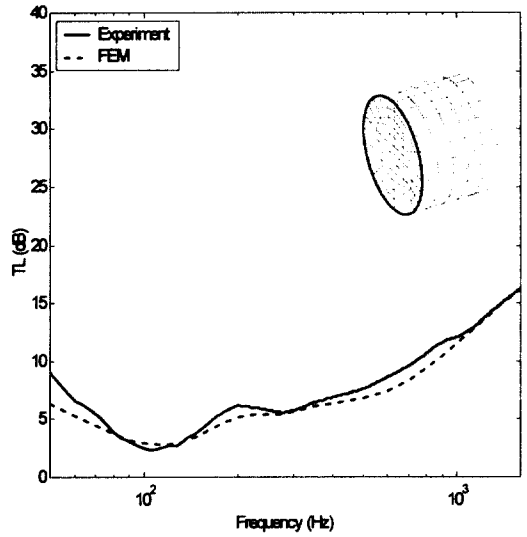

Figure 2 (a). Transmission loss of sample B constrained around edge.

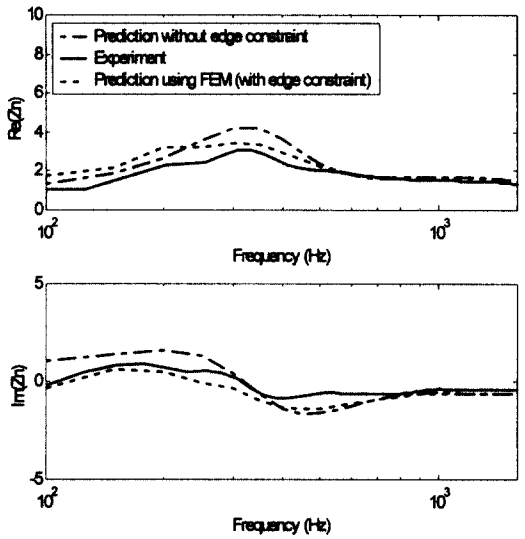

Figure 2 (b). Surface normal impedance of sample B constrained around edge.

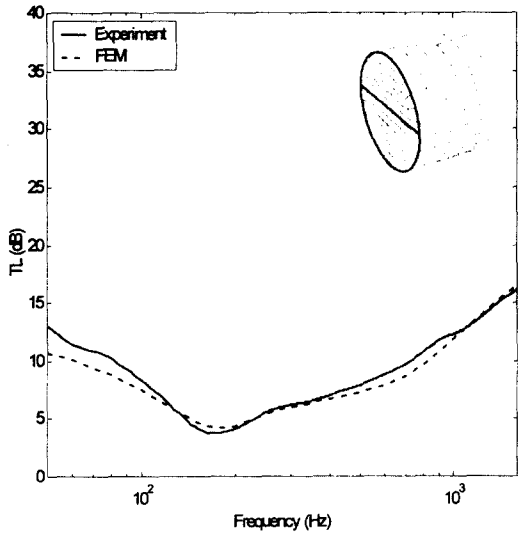

Figure 3 (a). Transmission loss of sample B constrained along plane.

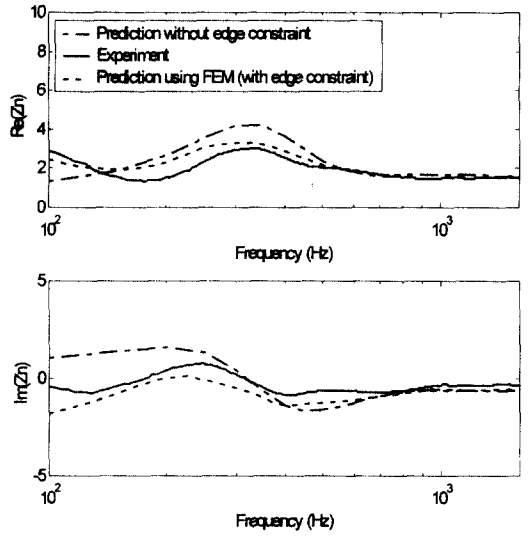

Figure 3 (b). Surface normal impedance of sample B constrained along plane.

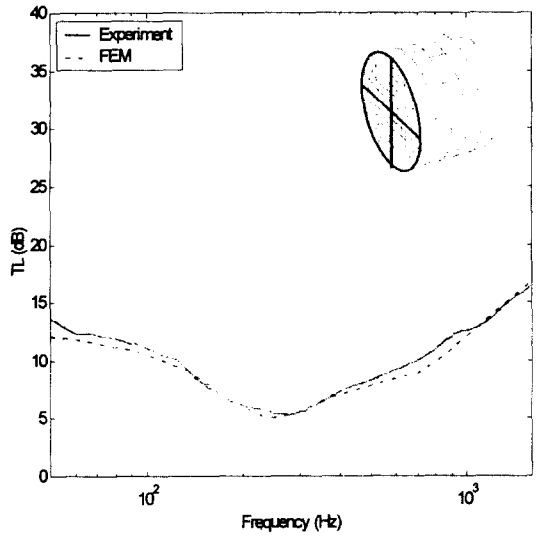

Figure 4 (a). Transmission loss of sample B constrained on cross.

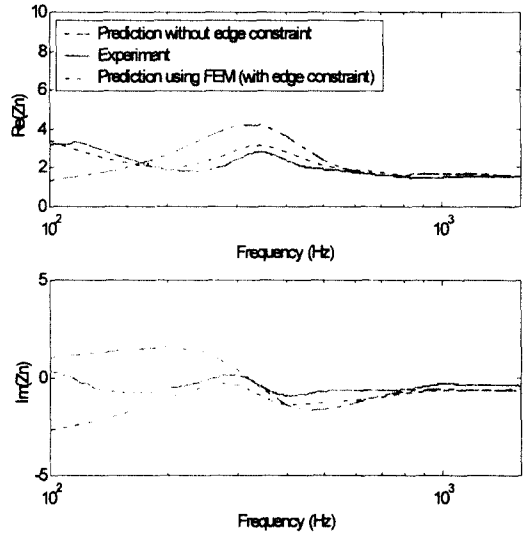

Figure 4 (b). Surface normal impedance of sample B constrained on cross.

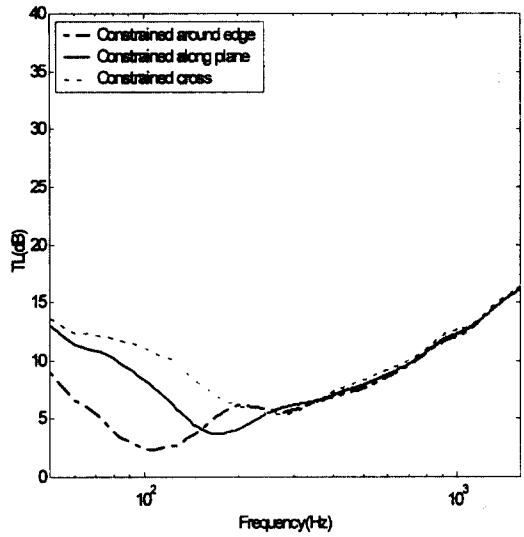

Figure 5 (a). Measured transmission loss.

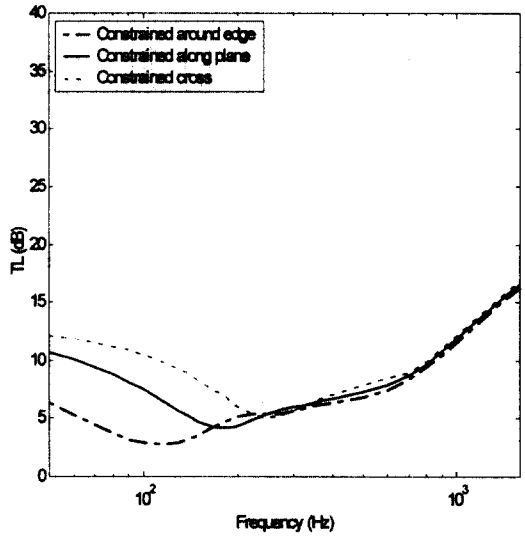

Figure 5 (b). Predicted transmission loss (FEM).

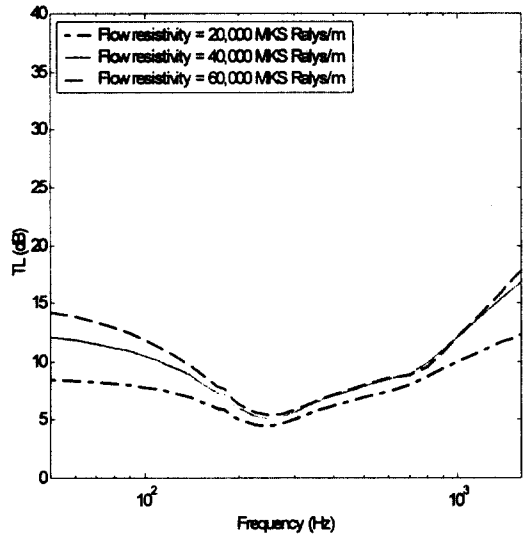

Figure 6. Effect of flow resistivity on TL for constrained cross case.

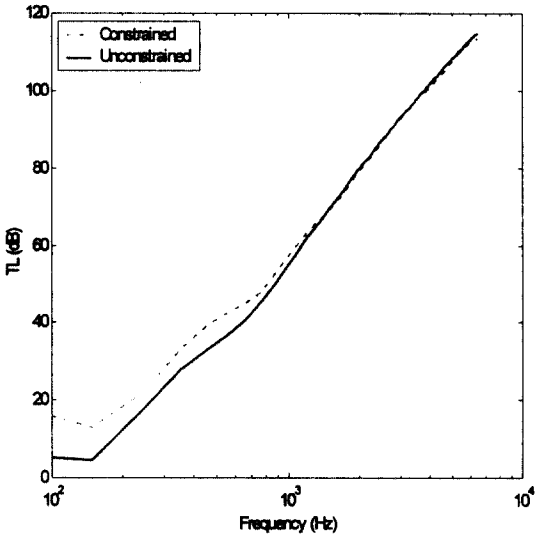

Figure 7. Transmission loss of double panel system lined with glass fiber for constrained case and unconstrained case.